Bioceramics

FABRICATION OF HYDROXYAPATITE–CALCITE NANOCOMPOSITE

E.K. Girija[a], G. Suresh Kumar[a], A. Thamizhavel[b], Y. Yokogawa[c], S. Narayana Kalkura[d]

[a]Department of Physics, Periyar University, Salem 636 011, India
[b]Department of Condensed Matter Physics, Tata Institute of Fundamental Research, Colaba, Mumbai 400 005, India
[c]Graduate School of Engineering, Department of Intelligent Materials Engineering, Osaka City University, Osaka 558 8585, Japan
[d]Crystal Growth Centre, Anna University, Chennai 600 025, India

ABSTRACT

Hydroxyapatite (HA) and calcite are known natural biomineral. HA is known to be bioactive and bioresorbable but the rates are too low. On the other hand, calcite is highly biodegradable. The combination of HA and $CaCO_3$ can compromise the demerits of each others. Here a method is presented for the simultaneous synthesis of HA and calcite employing sol-gel process. The product obtained was a nanocomposite with enhance bioactivity and elastic constants and fracture toughness similar to that of HA.

INTRODUCTION

Biological hard tissues are bio-composites of inorganic mineral with complex organic matrix. The inorganic minerals found in hard tissues of living organism include hydroxyapatite (HA), calcite, silica, magnetite etc.[1,2] Biomedical applications such as guided tissue regeneration, bone repair, drug delivery, tissue engineering etc requires smart biomaterial with multifunctions. There is a large demand for synthetic bone replacement materials. Materials with biocompatibility, bioactivity and bioresorbability are needed for making bone substitutes. Tissue engineering has the potential to create and regenerate tissues and organs and it requires coherent scaffold materials which can resorb at the rate of new bone regeneration.[1,2] Natural and synthetic hydroxyapatite is being investigated intensely with the aim of bone tissue engineering.[1-3] The resorption kinetics of HA is too low. Hence the biphasic mixture of HA and tricalcium phosphate has been studied by several researchers.[4] HA-calcite composite can be a more promising choice for this purpose as calcite is biocompatible, highly resorbable and can establish a direct bond with bone.[5,6] In this work, we report the simultaneous synthesis of HA-calcite nanocomposite by sol-gel method and their bioactivity and mechanical properties.

EXPERIMENTAL

Synthesis

Calcium nitrate tetrahydrate ($Ca(NO_3)_2{\cdot}4H_2O$, 98%), di-ammonium hydrogen phosphate ($(NH_4)_2HPO_4$, 99%), citric acid monohydrate ($C_6H_8O_7.H_2O$, 99.5%) and ammonia solution (NH_4OH, 25%) were used for the synthesis. The chemicals used were obtained from Merck and used without further purification. Deionized water was employed as the solvent. 1 M $Ca(NO_3)_2{\cdot}4H_2O$ and 0.6 M $(NH_4)_2HPO_4$ solutions were separately brought to pH above 10 with concentrated NH_4OH.[7] The calcium nitrate solution was stirred vigorously and di-ammonium hydrogen phosphate solution was added dropwise into it and stirred for 24 h at 60°C and the sample was named as A. The same experiment was also carried out in the presence of 1M citric acid at 60°C and the corresponding sample was referred as B. Both the as formed samples A and B were dried at 110°C for 48 h in air oven. Finally the samples were calcined at 400°C for 3 h and 1100°C for 10 h in a muffle furnace in open air atmosphere.

Characterization

XRD pattern of all synthesized and calcined samples were carried out using PANalytical X' Pert PRO diffractometer, with voltage and current setting of 40 kV and 30 mA, respectively. The XRD patterns were recorded in the range $20° \leq 2\theta \leq 60°$ at a scan speed of 1°/min giving a step size 0.0170° with Cu Kα radiation (1.5406 Å). Crystallographic identification of the phases of synthesized samples was accomplished by comparing the experimental XRD pattern with standard data compiled by the International Center for Diffraction Data (ICDD). The lattice parameters such as *a, c* and *V* were calculated by using method of least square.[8] The average particle size was calculated from XRD data using the Debye-Scherrer approximation[8]

$$D_{hkl} = \frac{K\lambda}{\beta_{1/2}\cos\theta}$$

where D_{hkl} is the particle size, as calculated for the (h k l) reflection, λ is the wavelength of CuKα radiation (1.5406 Å), $\beta_{1/2}$ is the full width at half maximum for the diffraction peak under consideration (in radian), θ is the diffraction angle (in degree) and K is the broadening constant chosen as 0.9. The diffraction peak at $2\theta = 25.8°$ was chosen for calculation of the particle size because it was sharper and isolated from others which is (002) Miller's plane of the hydroxyapatite crystal.

The degree of crystallinity (Xc) can be evaluated by the following equation[8,9]

$$X_c = \left(\frac{0.24}{\beta_{002}}\right)^3$$

where β_{002} is the full width at half maximum (degree) of (002) Miller's plane. The phase composition of synthesized samples was determined by the following equation[10]

$$RC_i = \frac{I(hkl)_i}{\sum I(hkl)_i}$$

where i and $I(hkl)_i$ refer to the phase of interest and intensity of the characteristic peaks of the corresponding phase, respectively, in the XRD pattern. $\Sigma I(hkl)_i$ is the total intensity of the characteristic peaks of the phases appeared in the XRD pattern. The HA powder samples calcined at 400°C were examined by FT–IR spectroscopy with Avatar 330 spectrometer (Thermo Nicolet, USA). The spectrum was recorded in the 4000–400 cm^{-1} region with 4 cm^{-1} resolution by using KBr pellet technique. The thermal behavior of the as-synthesized samples were determined by TG/DSC analyzer (NETZSCH, Germany) under Ar atmosphere using Al_2O_3 crucible with 20°C/min heating rate in the temperature from 25°C to 1000°C.

Bioactivity test

Bioactivity is the ability of the material to directly bond to bone through chemical interaction and not physical or mechanical attachment. Bioactivity has been characterized *in vitro* as the ability of the material to form carbonate apatite (similar to bone apatite) on its surface. The bioactivity of sample A (HA) and B (HA-calcite composite) were studied by immersing the compacted samples (pellets) in simulated body fluid (SBF) at 37°C. The SBF was prepared by dissolving appropriate amount of reagent grade NaCl, $NaHCO_3$, KCl, $Na_2HPO_4.H_2O$, $MgCl_2.6H_2O$, Na_2SO_4, $(CH_2OH)_3CNH_2$ and $CaCl_2.H_2O$ in deionized water. 1M HCl was used to maintain pH of the solution to 7.4 at 37°C to mimic the human plasma.[11] Then, the pellet samples were immersed in 30 ml of SBF in plastic containers with airtight lids and maintaining the temperature at 37°C in incubator. The SBF solution was renewed once in three days and pellet samples were immersed for a period of 21 days. The pH of the SBF solution was also measured during every renewal. Finally, the sample surface was analyzed by scanning electron microscope (SEM, JEOL-6390).

Density and porosity measurements

The density of the compacted samples were calculated using Archimede's principle by first measuring its mass, then its volume and dividing the mass by the volume. The samples were precision weighed in an electronic balance (Shimadzu Corporation, Japan) to an accuracy of 0.1 mg. The porosity of the samples was calculated by using the following relation

$$\text{Porosity} = \left(1 - \frac{\text{Measured density of sample}}{\text{Theoretical density of sample}}\right) \times 100$$

The theoretical density of samples was calculated by considering the theoretical density HA (3.16 g/cm^3) and calcite (2.71 g/cm^3) using law of mixture.[12]

Mechanical properties

We employed a non-destructive ultrasonic technique to measure the elastic constants of the samples.[13] The ultrasonic velocity (both longitudinal and shear direction) measurements were carried out using a high-power ultrasonic pulse receiver system (Fallon Ultrasonic Inc., Canada) with a 100 MHz digital storage oscilloscope (HP-54600B) using the cross-correlation technique described elsewhere.[13] Precise transit time for the propagation of the ultrasonic waves into the samples was measured by taking the difference in the transit times (Δt) between t_1 and t_2, where t_1 is the transit time measured only with buffer rods at a given temperature and t_2 is the transit time measured after introducing the sample in between the buffer rods, at the same temperature by using the following relation

$$U = \frac{\Delta t}{d}$$

where d is the thickness of samples. Elastic (longitudinal (L), shear (G) and Young's (E)) moduli and Poisson's ratio (σ) of the samples was calculated from the measured ultrasonic velocities (U_L and U_S) and density using the following relations. [13]

$$\text{Longitudinal modulus, } L = U_L^2 \rho$$

$$\text{Shear modulus, } G = U_S^2 \rho$$

$$\text{Poisson's ratio, } \sigma = \frac{(L - 2G)}{2(L - G)}$$

$$\text{Young's modulus, } E = (1+\sigma)2G$$

To determine the Vicker's hardness value, compacted samples (pellets) were subjected to a load of 200 g for 15 s with a Vicker's indenter (Micro Hardness Tester, HMV-2 Series, Shimadzu Corporation, Japan). A total of 3 indentations were made and the hardness values were averaged and reported. Vicker's hardness was calculated by using the following equation[14]

$$\text{Vicker's hardness, } H_V = 1.844 \times \frac{P}{d^2}$$

where P –Load (Kgf), d- Length of the diagonal of Vicker's indent. The fracture toughness K_C of the samples can be calculated using the following equation[14]

$$\text{Fracture toughness } K_C = 0.016\left(\frac{E}{H}\right)^{0.5}\left(\frac{P}{C^{1.5}}\right)$$

where E – Young's modulus (GPa), H – Vicker's hardness (GPa), P - Load (Kgf), C - Sum of half diagonal of Vicker's indent and crack length emanating from the corner of the Vicker's indent (mm).

RESULTS AND DICUSSIONS

XRD patterns of the as-synthesized gel powders are given in Fig. 1. Comparison of these patterns with JCPDS files conformed that the sample A is HA (JCPDS file No. 09–0432) with ammonium nitrate (JCPDS file No. 85–1093) and sample B contains minor quantity of β–TCP (JCPDS file No. 09–0169) and ammonium nitrate.

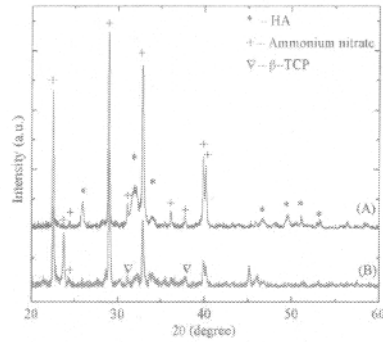

Fig.1. XRD patterns of the as-synthesized powders.

The XRD patterns of 400°C calcined samples showed the presence of pure HA in A and HA with an additional phase calcite (JCPDS file No. 47–1743) in B. The phase composition of HA and calcite in sample B was 76% and 22% respectively. When citric acid was introduced into the reaction medium it chelated with Ca ions and form Ca-citrate complex. Since the working pH was above 8 Ca-citrate formations was not much favored.[15] Only less amount of citrate ions complexed with Ca ions. The condition prevailed was favorable for the calcium phosphate formation. Hence in the as prepared sample trace amount of β–TCP existed and rest of the calcium phosphate may be in the amorphous form. Poorly crystalline HA phase has evolved along with calcite on 400°C calcination. The less amount of Ca-citrate existed in the as-synthesized powder has reacted with atmospheric oxygen and formed calcite according to the following reaction[16]

$$(C_6H_5O_7)_2Ca_3 + 9O_2 \quad 3CaCO_3 + 9CO_2 + 5H_2O$$

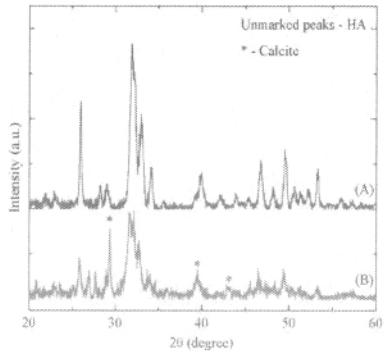

Fig.2. XRD patterns of samples calcined at 400°C.

Table 1 The crystalline parameters of HA powder calcined at 400°C.

Sample code	Lattice parameter (Å)		Average crystallite size D_{hkl} (nm)	Unit cell volume V ($Å^3$)	Lattice distortion c/a	Degree of crystallinity X_C
	$a = b$	c				
A	9.4238	6.8764	84	528.86	0.7296	15.6
B	9.4285	6.8808	55	529.73	0.7297	04.3

Table 1 gives the calculated values of crystalline parameters of samples calcined at 400°C. Existence of citric acid slightly increased the lattice parameters of HA. Crystallinity and average crystallite size was significantly reduced when citric acid was added during the synthesis. The free citrate ions existed in the medium might adsorb onto the precipitated amorphous calcium phosphate particles and would have controlled the size of particles. This might be the reason for the reduced crystllite size than the control samples.[17]

XRD patterns of samples calcined at 1100°C are shown in Fig. 3. On calcination at 1100°C HA has partially decomposed into oxyapatite (JCPDS file No. 89–6495) and β–TCP. Calcite has decomposed into CaO (JCPDS file No. 04–0777). The Phase composition of both samples calcined at 1100°C is shown in Table 2. The other phases such as oxyapatite, β–TCP and CaO formed when calcined at 1100°C indicate the thermal instability of the products synthesized.

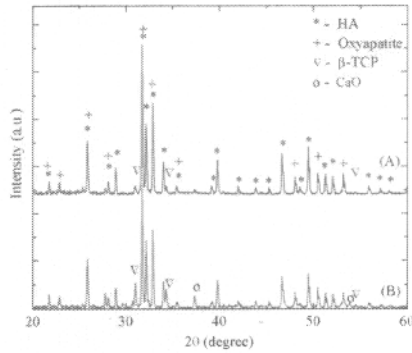

Fig. 3. XRD patterns of samples calcined at 1100°C.

Table 2 Phase composition of both samples calcined at 1100°C.

Sample code	Phase composition (%)			
	HA	Oxyapatite	β–TCP	CaO
A	49.3	49.3	1.4	-
B	41.7	41.7	11.3	5.3

The FT–IR spectra of samples calcined at 400°C are shown in the Fig. 4. All the four different vibrational modes of PO_4^{3-} were observed in the FT-IR spectra. The characteristic v_4 peaks of HA present at 575–610 cm^{-1} and the characteristic vibrational modes of OH group of HA at 3570 cm^{-1} and 628 cm^{-1} confirmed the phase formed to be HA.[6,7,18] The peaks present at 875 cm^{-1}, 1415 cm^{-1} and 1459 cm^{-1} in FT–IR spectra of samples A and B are attributed to the CO_3^{2-} ions. The FT-IR spectra of sample B showed all the above mentioned peaks but the CO_3^{2-} ion absorption peaks were stronger and wider than those for the sample A suggesting that there are more CO_3^{2-} groups present in these

samples. The existence of lattice water in both the samples was confirmed from the strong band at 1630–1636 cm^{-1} and a broad band between 3550–3200 cm^{-1}.[1, 6, 7, 18]

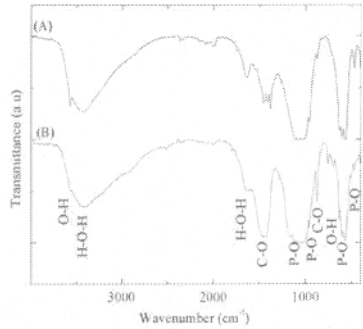

Fig. 4. FT–IR spectra of samples calcined at 400°C.

Fig. 5 shows the DSC trace of both samples. The endothermic peak around 100°C observed in A and B is due to the evaporation of adsorbed water.[6,7] With increasing temperature, an endothermic peak around 310°C and an exothermic peak around 313°C were found in A. These endothermic and exothermic peaks are attributed to the decomposition of ammonium nitrate in the as-prepared samples. The decomposition of ammonium nitrate takes place according to the following reactions

$$NH_4NO_3 \quad NH_{3\,(g)} + HNO_{3\,(g)} \text{ (Endothermic reaction)}$$

$$NH_4NO_3 \quad N_2O_{\,(g)} - 2H_2O_{(g\,)} \text{ (Exothermic reaction)}$$

These two reactions take place simultaneously during the decomposition of ammonium nitrate and the gaseous byproducts were readily evolved.[6,7] In B, along with ammonium nitrate decomposition of residual citric acid and calcium citrate takes place which has resulted in broad endothermic peak around 230°C and a very sharp intense exothermic peak at 290°C. A minute endothermic fall that occurs in DSC trace of sample B around 900°C could be attributed to the decorboxylation of samples, releasing CO_2.

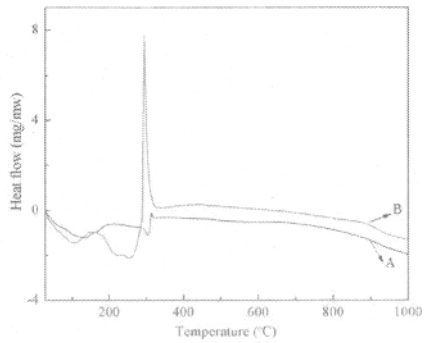

Fig. 5. DSC curve of as-synthesized gel powders.

TG curve of as-prepared samples is shown in Fig. 6. Both samples showed approximately 4–6% weight loss around 100°C, which is due to desorption of adsorbed water.[6,7] With increasing temperature, a weight loss of about 55% for sample A was observed between 100 and 300°C, which corresponded to the decomposition of ammonium nitrate. In case of samples B, a weight loss of about 70% was observed between 100 and 300°C which are attributed to decomposition of citric acid and ammonium nitrate. A weight loss about 10% was observed in between 280°C and 1000°C may be due to the slow release of CO_2.

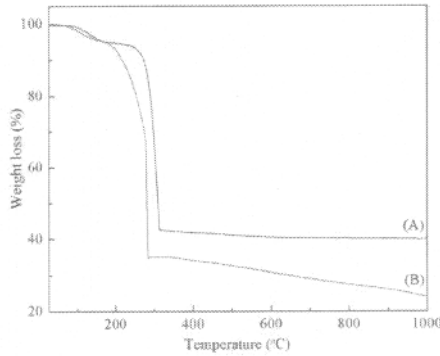

Fig. 6. TG curve of as-synthesized gel powders.

Fig. 7 and 8 shows the SEM images of the surfaces of sample A (HA) and sample B (HA-calcite composite) before and after soaking in SBF for 21 days. The surface of HA after soaking in SBF had shown the formation of spherical apatite particles of diameter >1μm on the surface. But the number of spherical deposits formed and the surface coverage was less. On the other hand, the surface of HA-calcite composite formed large number of clusters of spherical deposits and the surface was largely covered with such deposits. The inset in the figures shows the magnified view of the spherical deposit which depicts the flaky nano HA crystals constituting the spherical deposits. The pH of the SBF solution decreased during immersion of the pellets and the decrease was more for the HA-calcite composite. The consumption of OH ions from the solution to form the apatite on the surface of the pellet is the reason for the reduction in pH. The high bioactive nature of the HA-calcite composite is obvious from this study.

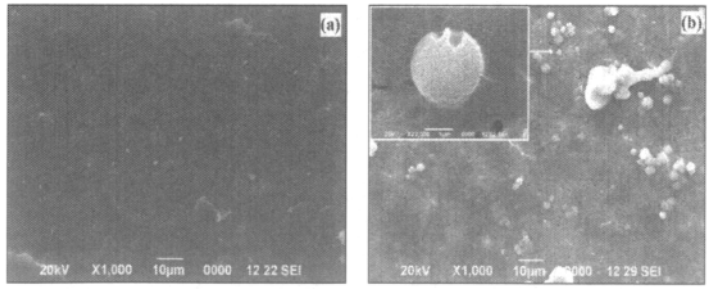

Fig. 7. SEM photograph of the surface of sample A (a) before and (b) after soaking in SBF.

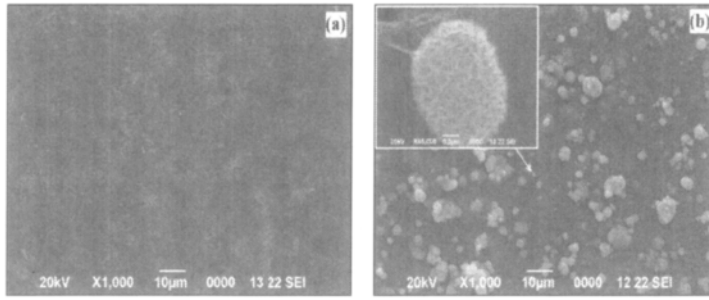

Fig. 8. SEM photograph of the surface of sample B (a) before and (b) after soaking in SBF.

The density, porosity and mechanical properties of both samples are given in Table 3. The samples prepared without citric acid (A) yielded high density than that of samples prepared in the presence of citric acid (B). The presence of calcite phase in the sample B significantly reduces the density of sample B due to its lower theoretical density than pure HA. However, mechanical properties did not get affected significantly due to presence calcite phase along with HA.

Table 3. Density, porosity and mechanical properties of samples.

Sample code	Density, (g/cm^3)	Porosity (%)	Longitudinal velocity, U_L (ms^{-1})	Shear velocity, U_S (ms^{-1})	Longitudinal modulus, L (GPa)	Shear modulus, G (GPa)	Poisson's ratio,	Young's modulus, E (GPa)	Hardness, H (GPa)	Fracture toughness, K_C ($MPa.m^{1/2}$)
A	2.30	27	2729	1654	17.12	06.29	0.209	15.20	1.029	0.37
B	2.27	22	2721	1673	16.80	06.35	0.196	15.18	0.637	0.38

CONCLUSIONS

Colloidal mixture of calcium and phosphate precursor followed by 110°C drying and 400°C calcination has resulted in HA phase with increased crystallite size in the case of control experiments and a nanocomposite of HA and calcite with reduced crystallite size in the citric acid used experiments. The citric acid introduced into the reaction medium has chelated with Ca ions resulting in the formation of calcite along with HA on 400°C calcinations. Citric acid has also reduced the crystallite size of HA. This HA–calcite nanocomposite showed higher bioactivity than HA which may due to dissolution of Ca ions from calcite in SBF. However, the presence of calcite along with HA neither improved nor reduced the mechanical properties.

ACKNOWLEDGMENTS

The authors (G.S and E.K.G) express their sincere thanks to Department of Science and Technology (DST), New Delhi, India (Project Ref. No: SR/FTP/PS-24/2009) for financial support.

REFERENCES

[1]S.V. Dorozhkin, Bioceramics of calcium orthophosphates, *Biomaterials*, **31**, 1465-1485 (2010).

[2]S.J. Kalita, A. Bhardwaj, H.A. Bhatt, Nanocrystalline calcium phosphate ceramics in biomedical engineering, *Mater. Sci. Eng. C*, **27**, 441-449 (2007).
[3]W. Suchanek, M. Yoshimura, Processing and properties of hydroxyapatite-based biomaterials for use as hard tissue replacement implants, *J. Mater. Res.*, **13**, 94-116 (1998).
[4]R.Z. LeGeros, S. Lin, R. Rohanizadeh, D. Mijares, J.P. LeGeros, Biphasic calcium phosphate bioceramics: preparation, properties and applications, *J. Mater. Sci.: Mater. Med.*, **14**, 201-209 (2003).
[5]Y. Fujita, T. Yamamuro, T. Nakamura, S. Kotani, The bonding behavior of calcite to bone, *J. Biomed. Mater. Res.*, **25**, 991-1003 (1991).
[6]G.S. Kumar, E.K. Girija, A. Thamizhavel, Y. Yokogawa, S.N. Kalkura, Synthesis and characterization of bioactive hydroxyapatite-calcite nanocomposite for biomedical applications, *J. Colloid Interface Sci.*, **349**, 56-62 (2010).
[7]E. Hayek and H. Newesely, Pentacalcium Monohydroxyorthophosphate, *Inorg. Synth.*, 7, 63-65 (1963)
[8]F. Ren, R. Xin, X. Ge, Y. Leng, Characterization and structural analysis of zinc-substituted hydroxyapatites, *Acta Biomater.*, **5**, 3141-3149 (2009).
[9]E. Landi, A. Tampieri, G. Celotti, S. Sprio, Densification behaviour and mechanisms of synthetic hydroxyapatites, *J. Eur. Ceram. Soc.*, **20**, 2377-2387 (2000).
[10]C. Ergun, Effect of Ti ion substitution on the structure of hydroxylapatite, *J. Eur. Ceram. Soc.*, **28**, 2137-2149 (2008).
[11]A.C. Tas, Synthesis of biomimetic Ca-hydroxyapatite powders at 37°C in synthetic body fluids, *Biomaterials*, **21**, 1429-1438 (2000).
[12]Y. Hu, X. Miao, Comparison of hydroxyapatite ceramics and hydroxyapatite/borosilicate glass composites prepared by slip casting, *Ceram. Int.*, **30**, 1787-1791(2004).
[13]O. Prokopiev, I. Sevostianov, Dependence of the mechanical properties of sintered hydroxyapatite on the sintering temperature, *Mater. Sci. Eng. A*, **431**, 218-227 (2006).
[14]J. Wang, L.L. Shaw, Nanocrystalline hydroxyapatite with simultaneous enhancements in hardness and toughness, *Biomaterrials*, **30**, 6565-6572 (2009).
[15]M.A. Martins, C. Santos, M.M. Almeida, M.E.V. Costa, Hydroxyapatite micro- and nanoparticles: Nucleation and growth mechanisms in the presence of citrate species, *J. Colloid Interface Sci.*, **318**, 210-216 (2008).
[16]A.I. Mitsionis, T.C. Vaimakis, C.C. Trapalis, The effect of citric acid on the sintering of calcium phosphate bioceramics, *Ceram. Int.*, **36**, 623-634 (2010).
[17]C. L. Chu, P.H. Lin, Y. S. Dong, D.Y. Guo, Influences of citric acid as a chelating reagent on the characteristics of nanophase hydroxyapatite powders fabricated by a sol-gel method, *J. Mater. Sci. Lett.*, **21**, 1793-1795 (2002).
[18]S. Koutsopoulos, Synthesis and characterization of hydroxyapatite crystals: A review study on the the analytical methods, *J. Biomed. Mater. Res.*, **62**, 600-612 (2002).